Computational Design of Active Site Structures with Improved Transition-State Scaling for Ammonia Synthesis

Aayush R. Singh,[†] Joseph H. Montoya,[†] Brian A. Rohr,[†] Charlie Tsai,[†] Aleksandra Vojvodic,[‡,¶] and Jens K. Nørskov[*,†,‡]

† *SUNCAT Center for Interface Science and Catalysis, Department of Chemical Engineering, Stanford University, Stanford, California, 94305, USA*

‡ *SUNCAT Center for Interface Science and Catalysis, SLAC National Accelerator Laboratory, Menlo Park, California, 94025, USA*

¶*Department of Chemical and Biomolecular Engineering, University of Pennsylvania, Philadelphia, Pennsylvania, 19104, USA*

E-mail: norskov@stanford.edu

Abstract

The Haber-Bosch process for the reduction of atmospheric nitrogen to ammonia is one of the most optimized heterogeneous catalytic reactions, but there are aspects of the industrial process that remain less than ideal. It has been shown that the activity of metal catalysts is limited by a Brønsted-Evans-Polanyi (BEP) scaling relationship between the reaction and transition-state energies for N_2 dissociation, leading to a negligible production rate at ambient conditions and a modest rate under harsh conditions. In this study, we use density functional theory (DFT) calculations in conjunction with mean-field microkinetic modeling to study the rate of NH_3 synthesis on model active

sites that require the singly-coordinated dissociative adsorption of N atoms onto transition metal atoms. Our results demonstrate that this "on-top" binding of nitrogen exhibits significantly improved scaling behavior, which can be rationalized in terms of transition-state geometries, and leads to considerably higher predicted activity. While synthesis of these model systems is likely challenging, the stabilization of such an active site could enable thermochemical ammonia synthesis under more benign conditions.

Keywords: ammonia synthesis, density functional theory, microkinetic modeling, transition-states, scaling relations

1 Introduction

Ammonia (NH_3) plays a crucial role in large-scale fertilizer production, which has allowed the global population to explode from 1.6 billion in 1900 to more than 7 billion today.[1] The Haber-Bosch process for the reduction of atmospheric nitrogen to ammonia, $N_2 + 3H_2 \rightarrow 2NH_3$, has been named the most important invention of the 20th century, and the current estimated yearly industrial production of 500 million tons of NH_3, at the cost of 1% of the planet's energy consumption and 3-5% of the global natural gas supply,[2] attests to ammonia's continued importance in the modern world economy.

The Haber-Bosch process is among the most-studied and best-understood heterogeneous catalytic reactions. Although a long history of experimental and theoretical studies has identified N_2 dissociation as the rate-limiting step for the reaction,[3–9] and has led to a well-optimized process catalyzed by transition metal surfaces, significant drawbacks remain that still need to be addressed. A density functional theory (DFT) free energy analysis of the intermediate steps and activation barriers[10] by Vojvodic *et al.* reveals that key intermediates such as *N, *NH, and *NH_2 bind too strongly to the most common metal catalyst surfaces (Fe, Ru) under ambient conditions (300 K and 1 bar), preventing the reaction from proceed-

ing. An appreciable number of free active sites can be generated by raising the temperature to 700 K, but this temperature increase must be coupled with a significant pressure increase on the order of 100 bar to keep the overall reaction exergonic. These harsh conditions make the industrial Haber-Bosch process highly capital-intensive, and thus fertilizer is generally produced in large, centralized factories. An important disadvantage of this scheme is that the overall efficiency of production, delivery, and uptake of fertilizer by crops is quite low, and the price of fertilizer at the point of use is prohibitively high in many places around the world.[11] It could be both economically and environmentally advantageous to find an alternative route for producing ammonia at ambient temperatures and pressures, in small-scale devices based on sustainable energy sources such as photovoltaics and wind.

The thermodynamic limitations of the Haber-Bosch process under ambient conditions could in theory be circumvented by finding a catalyst that binds $*NH_x$ (x = 0, 1, or 2) more weakly than, for example, a stepped Ru surface without increasing the barrier for N_2 dissociation. DFT calculations have shown, however, that a Brønsted-Evans-Polanyi (BEP) scaling relation for transition metal stepped transition metal surfaces prevents the N-N transition-state energy (E_{N-N}) from being varied independently of the *N binding energy to the surface (E_N).[12,13] The best catalyst of this class of materials must therefore find the ideal balance between E_{N-N} and E_N while satisfying the BEP scaling line constraint. Previous microkinetic analyses have shown that for stepped surfaces, the best ammonia synthesis catalysts known today, E_{N-N} is consistently too high relative to E_N, leading to a negligible production rate at ambient conditions and a modest rate under elevated temperatures and pressures.[10]

In light of the thermodynamic and kinetic limitations described above, the task of designing better thermochemical ammonia synthesis catalysts can be reduced to finding a class of materials with better transition-state scaling for N_2 dissociation. BEP scaling for this reaction could conceivably be improved in the following two ways. The first approach involves

stabilizing the N-N transition-state relative to the dissociated final-state, perhaps through interactions inside of a porous (zeolite) material. The second approach requires de-stabilizing the dissociated *N state relative to the transition-state by, for example, forcing N_2 to dissociate onto a less stable active site than the three-fold step site traditionally found on transition metal surfaces. These two approaches correspond to moving the BEP scaling line downward and rightward, respectively, and both lead to an operating point on the activity map that is closer to optimal. It is important to note that the transition-state energy can never be lower than the final-state energy, and thus $E_{N-N} = 2E_N$ represents the ideal BEP scaling line (two N atoms bind to the surface for every dissociated N_2 molecule). Vojvodic *et al.* have shown that rutile oxide materials exhibit close-to-ideal BEP scaling for the dissociation of a variety of small molecules, including N_2.[10,14] This enhancement in scaling is attributed to the binding of N atoms onto less stable under-coordinated metal sites. Due to the significant de-stabilization of $*NH_x$ on rutile oxides compared to the stepped transition metal surfaces, however, there are no known oxides that bind $*NH_x$ strongly enough ($2E_N < 2$ eV) to produce ammonia at an appreciable rate. The identification of materials with BEP scaling like that of rutile oxide surfaces but moderate binding energies comparable to stepped transition metal surfaces could significantly improve the industrial Haber-Bosch process.

In the present study, we use DFT calculations to study the rate of ammonia synthesis on model active sites that explicitly force the singly coordinated dissociative adsorption of N atoms onto transition metal atoms, primarily by placing reactive metal atoms into the surface layers of otherwise unreactive metal lattices. Our results demonstrate that this "on-top" binding of nitrogen breaks the transition-state scaling relation that limits the activity of the industrially relevant transition metal step surfaces. These model systems, which span a large range of E_N values, exhibit close-to-ideal scaling for the most positive E_N values and deviations away from ideal scaling as E_N becomes more negative. We explain the deviations in scaling behavior in terms of transition-state geometry. While synthesis of these model

systems is likely challenging, we demonstrate through the example of a rhenium stripe in a copper (211) lattice that the stabilization of such an active site could lead to significantly lower pressure requirements for ammonia synthesis.

2 Computational Methods

Electronic structure calculations are performed using the Quantum Espresso Software package, implemented in the Atomic Simulation Environment (ASE).[15] The BEEF-vdW exchange correlation functional is used to accurately model adsorption energies and van der Waals interactions.[16] In all calculations, plane wave and density wave cutoffs of 500 eV and 5000 eV, respectively, are used, along with a 4x4x1 Monkhorst-Pack k-point grid.[17]

The "on-top" dissociation of N_2 is studied on a variety of different system geometries, hereafter known as "top-stable systems", to span a wide $2E_N$ space. One way to force this type of dissociation is to place small reactive transition metal clusters in otherwise unreactive lattices, where the lattice constants are optimized prior to doping the system with guest atoms. The locality of these reactive atoms leads to the singly-coordinated adsorption of N atoms because interaction with the surrounding lattice is, by design, unfavorable. To further expand the energy space considered, pure transition metal FCC (111) surfaces with N_2 dissociation restricted to the "on-top" site by a fixed-line constraint are also considered. A range of strains up to 5% in the tensile and compressive directions is applied parallel to the transition metal surfaces, such that the $2E_N$ value is varied systematically.[18] Finally, one set of known catalysts that bind N atoms in the "on-top" configuration are the metal edges of transition metal sulfides. Several sulfide systems are included to extend the results of the study to more realistic materials. Representative geometries for the various top-stable systems considered in the study are shown in Fig. 1. Most of the surfaces studied are 4 layers thick in the z-direction (Systems A, B, C, D, F, G, I, and J in Fig. 1), while System E is a

single-layered graphene sheet and System H consists of 3 layers. As shown by the representative unit cells in Fig. 1, most systems range from 2-4 atoms wide in the x and y directions, consistent with the typical rule of thumb that the product of the number of k-points and the unit cell dimension should be greater than 20 Å in each direction for metallic systems.[15,19] Table S1 of the Supporting Information provides a complete listing of the systems studied, including the geometry, identity of the reactive and unreactive atoms, and exposed crystal facet. Adsorbates and 0-1 surface layers are relaxed such that the maximum force on each atom is less than 0.05 eV/Å.

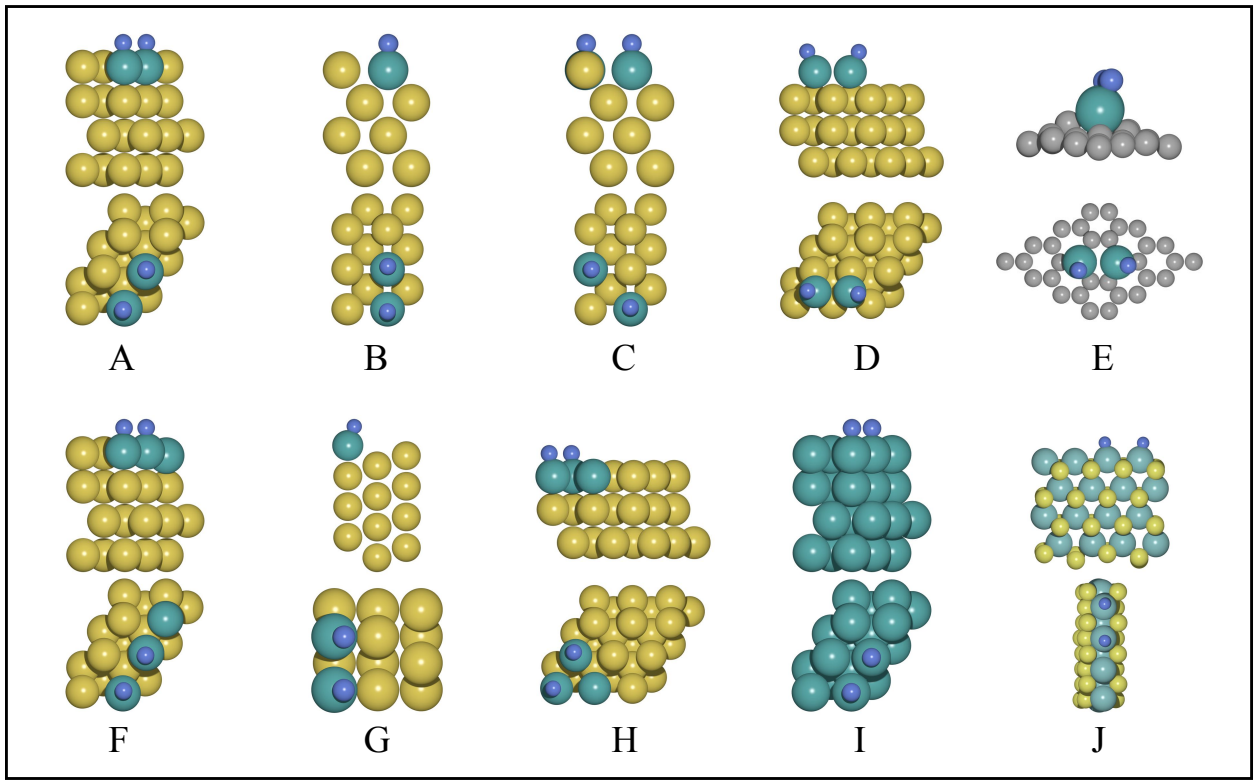

Figure 1: Representative top-view and side-view images of the top-stable active site geometries considered in this study. (A) Metal dimer doped in an FCC (111) surface. (B) (Adjacent) Metal dimer doped in an FCC (100) surface. (C) (Diagonal) Metal dimer doped in an FCC (100) surface. (D) Adatom dimer on an FCC (111) surface. (E) Metal dimer doped in a graphene lattice. (F) Metal stripe doped in an FCC (111) surface. (G) Metal stripe doped in an FCC (211) surface. (H) Metal trimer doped in an FCC (111) surface. (I) FCC (111) metal top site. (J) Metal sulfide metal edge.

Transition-state energies are determined by sampling the reaction path using a fixed-bond-length (FBL) constraint between the dissociating N atoms. The FBL method has been previously shown to compare favorably with the more computationally expensive Nudged Elastic Band (NEB) method for simple dissociation reactions.[20–22]

Calculated $2E_{\mathrm{N}}$ and $E_{\mathrm{N-N}}$ values for the top-stable systems studied are recorded in Table S1 of the Supporting Information. Barriers and reaction energies are then used as input into the CatMAP software,[23] which generates activity heatmaps corresponding to rates as a function of descriptor adsorption energies. Each adsorption energy is calculated from DFT as the electronic energy of an adsorbate on top of a slab minus the combined electronic energies of the empty slab and the associated gas phase reference molecules (in this case N_2 and H_2). Electronic energy differences are converted to free energies in CatMAP by adding corrections for zero-point energy (ΔZPE) and entropy (-TΔS) (in the harmonic approximation for adsorbates and using ideal gas thermochemistry as implemented in ASE).

It is important to note that the uncertainty associated with an individual material, especially in cases when the surface layer is not allowed to relax, is much greater than the uncertainty on the scaling line constructed from the large set of points in this study.[24] Finding the exact position of a given real material along the scaling line can require more detailed calculations than those performed here.

3 Results and Discussion

One of the simplest possible micro-kinetic models that can be considered for ammonia synthesis assumes that N_2 dissociation is the rate-determining step (RDS) for the process, an experimentally verified observation for industrial catalysts.[3–5] The kinetic reactions for this RDS model, similar to those employed by Medford *et al.*,,[25] are shown in Eqs. 1-2.

$$\mathrm{N_2(g)} + 2* \;\leftrightarrow\; \mathrm{N\text{-}N*} + * \;\rightarrow\; 2\mathrm{N*} \qquad \text{[RDS]} \tag{1}$$

$$\mathrm{N}* + \frac{3}{2}\mathrm{H_2(g)} \;\leftrightarrow\; \mathrm{NH_3(g)} + * \tag{2}$$

Assuming that Eq. 2 is quasi-equilibrated and that the total number of catalytic sites is fixed leads to the following analytical expression for the turnover frequency (TOF) (Eq. 3).

$$\mathrm{TOF} = k_1 P_{\mathrm{N_2}} \left(1 + \frac{P_{\mathrm{NH_3}}}{K_2 P_{\mathrm{H_2}}^{1.5}}\right)^{-2} \left(1 - \frac{P_{\mathrm{NH_3}}^2}{K_{\mathrm{tot}} P_{\mathrm{H_2}}^3 P_{\mathrm{N_2}}}\right) \tag{3}$$

The reaction rate constant k_1 for Eq. 1 can be computed from transition-state theory (TST) according to Eq. 4, while the equilibrium constants for Eq. 2 (K_2) and the overall reaction (K_{tot}) can be calculated as shown in Eqs. 5 and 6, respectively.

$$k_1 = \frac{k_{\mathrm{B}} T}{h} \exp\left(-\frac{\Delta G_{\mathrm{TS},1}}{k_{\mathrm{B}} T}\right) \tag{4}$$

$$K_2 = \exp\left(-\frac{\Delta G_{\mathrm{rxn},2}}{k_{\mathrm{B}} T}\right) \tag{5}$$

$$K_{\mathrm{tot}} = \exp\left(-\frac{\Delta G_{\mathrm{rxn},1} + 2\Delta G_{\mathrm{rxn},2}}{k_{\mathrm{B}} T}\right) \tag{6}$$

The above expression for TOF (Eq. 3) is written explicitly in terms of the pressure of the reactants and products *relative to the standard state pressure* (1 bar), such that the temperature-dependent rate constants and equilibrium constants need only be calculated at standard state.

Since the free energies of the reactants and products are set by a choice of reaction temperature and species pressures, and only the N_2 dissociation step is considered to be out of equilibrium, the TOF for the RDS model depends on exactly two independent *electronic* energy parameters: $E_{\mathrm{N-N}}$ (the transition-state energy for N_2 dissociation, equivalent to $\Delta E_{\mathrm{TS},1}$) and $2E_{\mathrm{N}}$ (the N_2 dissociation energy, equivalent to $\Delta E_{\mathrm{rxn},1}$). Medford *et al.*[25] have previously created a 2-D activity heatmap depicting TOF as a function of $2E_{\mathrm{N}}$ and $E_{\mathrm{N-N}}$ for

this model, assuming that the two variables can be varied independently of each other. They observed that the BEP scaling line for stepped transition metal surfaces is far away from the ideal scaling between $E_{\mathrm{N-N}}$ and $2E_{\mathrm{N}}$, given by $E_{\mathrm{N-N}} = 2E_{\mathrm{N}}$, which leads to sub-optimal NH_3 synthesis rates. The idea that a heatmap can be divided into regions of different activity levels using linear scaling constraints has also been previously discussed by Cheng *et al.*[26] The 2-D heatmap suggests that new catalysts satisfying the assumptions of the RDS model could lead to an improvement in TOF of more than 10 orders of magnitude if they exhibit closer-to-ideal scaling. While the assumption of N_2 dissociation being rate-limiting is likely to be reasonable for catalysts similar to the industrial state of the art, the validity of the RDS model for catalyst motifs that are closer to the peak of the activity heatmap has yet to be confirmed. Since a shift in scaling towards ideal would correspond to increasingly easier N_2 dissociation, it is possible that a later step in the reaction pathway could become rate determining. The continued use of the RDS model under improved BEP scaling for N_2 dissociation implicitly assumes that other steps in NH_3 synthesis also become simultaneously easier, such that N_2 dissociation still controls the overall rate.

In this study, we start by exploring the limits of the above model. While the RDS model adequately describes a limit in which all steps in the reaction pathway become comparably easier with an improvement in $E_{\mathrm{N-N}}$ vs. $2E_{\mathrm{N}}$ scaling, a more sophisticated model is needed to explore the case in which no other reaction steps are affected by a change in the N_2 dissociation barrier. The following steady-state (SS) model is used to describe such a system. The SS model reaction mechanism is shown in Eqs. 7-13.

$$\mathrm{N_2(g)} + * \;\leftrightarrow\; \mathrm{N_2}* \tag{7}$$

$$\mathrm{H_2(g)} + 2*_{\mathrm{h}} \;\leftrightarrow\; 2\mathrm{H}*_{\mathrm{h}} \tag{8}$$

$$\mathrm{N_2{*}} + {*} \;\leftrightarrow\; \mathrm{N\text{-}N{*}} + {*} \;\rightarrow\; \mathrm{2N{*}} \tag{9}$$

$$\mathrm{N{*}} + \mathrm{H{*}_h} \;\leftrightarrow\; \mathrm{N\text{-}H{*}} + {*_h} \;\rightarrow\; \mathrm{NH{*}} + {*_h} \tag{10}$$

$$\mathrm{NH{*}} + \mathrm{H{*}_h} \;\leftrightarrow\; \mathrm{NH\text{-}H{*}} + {*_h} \;\rightarrow\; \mathrm{NH_2{*}} + {*_h} \tag{11}$$

$$\mathrm{NH_2{*}} + \mathrm{H{*}_h} \;\leftrightarrow\; \mathrm{NH_2\text{-}H{*}} + {*_h} \;\rightarrow\; \mathrm{NH_3{*}} + {*_h} \tag{12}$$

$$\mathrm{NH_3{*}} \;\leftrightarrow\; \mathrm{NH_3(g)} + {*} \tag{13}$$

The model considers barrierless N_2(g) and H_2(g) adsorption onto two different sites, * and $*_h$, respectively, to simulate a hydrogen reservoir[27] on non-step sites of a nanoparticle. Transition-states are included explicitly for N_2 dissociation, as before, along with the surface hydrogenation of N*, NH*, and NH_2*. Desorption of NH_3* is also deemed to be barrierless. Barrierless in this context means no *additional* barrier beyond the reaction energy for a given step. All NH_x species are assumed to bind through the N atom on a * site. In addition to the two key parameters needed for the RDS model, $E_{\mathrm{N-N}}$ and $2E_{\mathrm{N}}$, the SS model requires the following other binding and transition-state energies for each catalyst: $E_{\mathrm{N_2}}$, E_{H}, $E_{\mathrm{N-H}}$, E_{NH}, $E_{\mathrm{NH-H}}$, $E_{\mathrm{NH_2}}$, $E_{\mathrm{NH_2-H}}$, and $E_{\mathrm{NH_3}}$.

In order to create a 2-D activity heatmap for comparison with the RDS model, linear intermediate and transition-state scaling relations for transition metal stepped surfaces are used to reduce the complexity of the model back down to the same two parameters, $E_{\mathrm{N-N}}$ and $2E_{\mathrm{N}}$. Other than N-N*, which is assumed to have an independent binding energy, all intermediates and transition-states binding to the surface through an N atom are assumed to scale linearly with $2E_{\mathrm{N}}$.[10,28,29] The binding energy of H* is also scaled with N*.[30]

A steady-state solution to Eqs. 7-13 is obtained by imposing that coverages of all intermediates are time-independent. The sum of coverages must also add up to 1 for each site type. These conditions are summarized in Eqs. 14-16.

$$2r_7 = \frac{2}{3}r_8 = 2r_9 = r_{10} = r_{11} = r_{12} = r_{13} \tag{14}$$

$$\theta_{\mathrm{N_2}} + \theta_{\mathrm{N}} + \theta_{\mathrm{NH}} + \theta_{\mathrm{NH_2}} + \theta_{\mathrm{NH_3}} + \theta_{*} = 1 \tag{15}$$

$$\theta_{\mathrm{H}} + \theta_{*_{\mathrm{h}}} = 1 \tag{16}$$

A 2-D activity heatmap displaying the steady-state TOF as a function of these two variables is shown in Fig. 2. The rates are calculated at a temperature of 673 K and a total pressure of 100 bar, with a stoichiometric ratio of H_2 to N_2 (3:1) and 10 percent conversion to NH_3. These conditions are meant to simulate the harsh conditions required industrially for the Haber-Bosch process. Also plotted are two BEP scaling lines. The upper dashed line corresponds to the stepped transition metal surfaces,[25] while the lower dashed line represents the ideal or theoretically optimal scaling line, where $E_{\mathrm{N-N}} = 2E_{\mathrm{N}}$. The region of the graph where $E_{\mathrm{N-N}} < 2E_{\mathrm{N}}$ is therefore unphysical. Qualitatively, the SS activity heatmap is similar to the RDS heatmap established by Medford *et al.*[25] Both activity heatmaps show that no stepped surface of a single transition metal exists at the top of the activity heatmap (with ruthenium and iron the closest, matching experiments), and that identifying catalysts closer to the ideal scaling line for N_2 dissociation would lead to significantly higher rates. Quantitatively, however, there are key differences between the heatmaps. While the peak rates of both maps occur at similar values of $2E_{\mathrm{N}}$ (slightly more negative than -1 eV), and the calculated rates along the stepped transition metal scaling line are comparable (peak rates on the order of 10^{-3} s^{-1}), the predicted increase in rate for a shift towards ideal scaling is substantially larger in the RDS case (more than 10 orders of magnitude) compared to

the SS case (around 3 orders of magnitude). This difference occurs because the RDS model assumes that N_2 dissociation continues to control the rate as E_{N-N} decreases, leading to a higher rate until either $E_{N-N} = 2E_N$ (the right side of the map) or the free energy barrier hits zero (the left side of the map). In contrast, the SS model provides a better description of catalysts with close-to-ideal scaling because it does not impose a rate-determining step, and as a result, allows other steps such as hydrogenation to become more important than N_2 dissociation, modulating the enhancement in activity that can be gained from improved transition-state scaling.

It is important to note that neither of the two models consider the effects of coverage or adsorbate-adsorbate interactions on the kinetics of ammonia synthesis. This means that both the SS and RDS models systematically over-estimate the effect of NH_x poisoning on the far left side of the activity heatmap. In reality, the rates of NH_3 production in the strong-binding region would be somewhat higher than predicted here, though still much lower than the most promising regions of the heatmap where good catalysts would be found. The inclusion of repulsive adsorbate-adsorbate interactions would likely also destabilize the final state of N_2 dissociation slightly more than the transition-state (since the dissociated 2N* state takes up two active sites), shifting the calculated scaling line slightly towards the ideal scaling line. These calculations can therefore be thought of as a conservative estimate for the true activity, and any conclusions about the qualitative improvement in transition-state scaling between different materials should not be significantly affected.

Calculated ($2E_N$,E_{N-N}) data points for numerous top-stable systems are plotted onto the SS activity heatmap in Fig. 3 . Panel A shows the full dataset, while panel B depicts a smaller energy space near the peak of the activity heatmap that contains the most promising candidate active sites. The stepped transition metal and ideal scaling lines are also shown for comparison. There is significant scatter in the data, but it is clear that neither of the two scaling lines shown are sufficient to describe the systems that have been investigated. A number of systems exhibit considerably better transition-state scaling for N_2 dissociation,

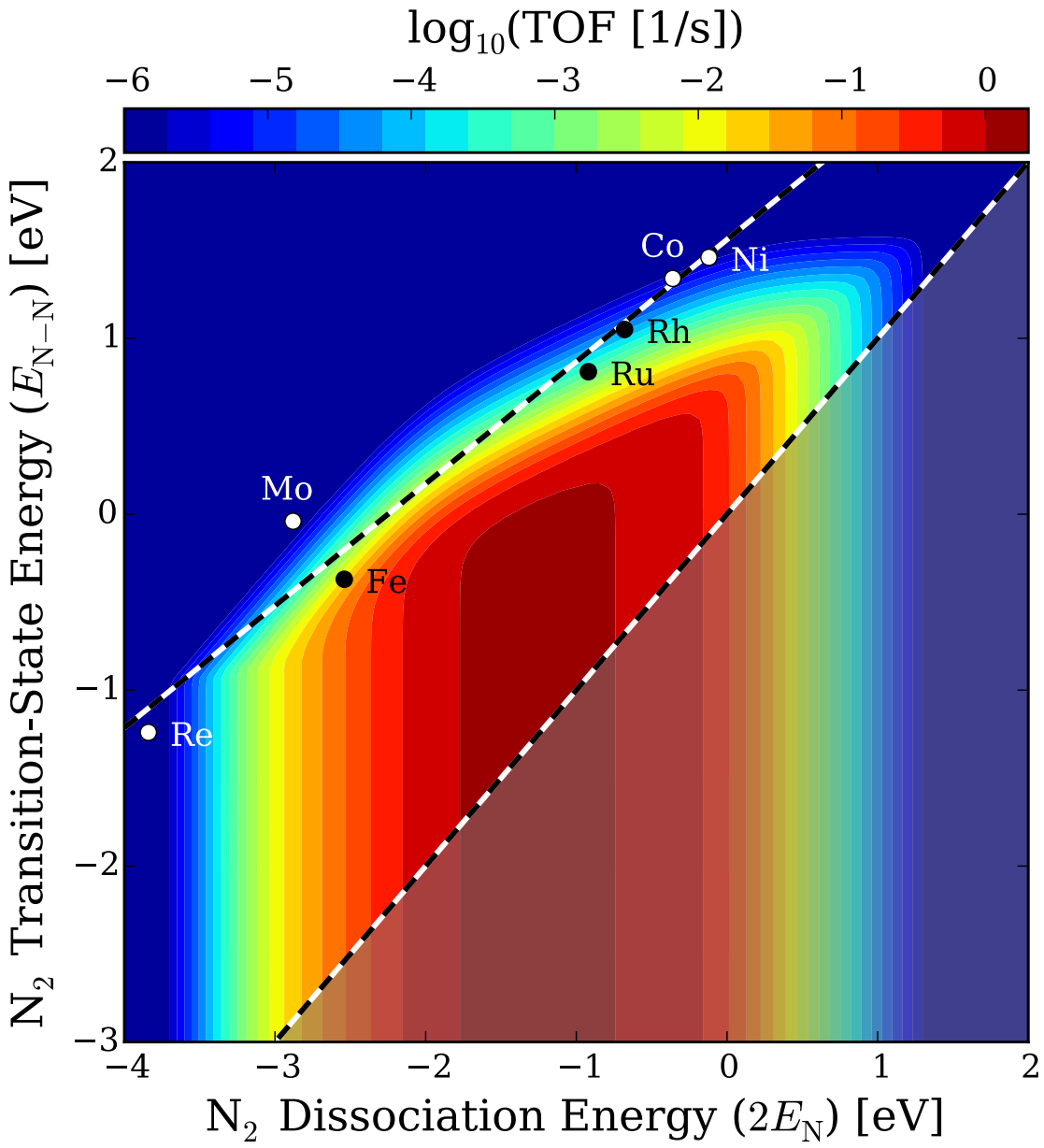

Figure 2: 2-D activity heatmap describing the steady-state TOF to NH_3 as a function of E_{N-N} and $2E_N$, computed at a temperature of 673 K, a total pressure of 100 bar, a stoichiometric ratio of H_2 to N_2 (3:1), and 10 percent conversion to NH_3. Two BEP scaling lines are shown (upper corresponding to stepped transition metal surfaces and lower corresponding to the ideal limit).

and therefore a much higher predicted ammonia synthesis rate. To explain the significant improvement in scaling for these catalysts, we once again invoke the premise of this work, which is that changing the bonding coordination of the dissociated nitrogen atoms from three-fold on a close-packed surface or four-fold on a stepped surface to one-fold coordination on these top-stable systems greatly reduces the binding strength of the N atoms. Since the transition-state geometries on stepped transition metal surfaces are already relatively under-coordinated compared to the fully dissociated final states, moving to a top-stable system has a smaller impact on the transition-state energy. A greater destabilization of the final-state compared to the transition-state leads to a rightward shift of the scaling line, an effect that is clearly seen in the data. It is important to note that since dissociation energies are being weakened by this scheme, transition metal atoms that generally bind NH_x species too strongly (*e.g.* Re and Mo) are now close to the optimal binding strength upon switching to singly-coordinated adsorption. Systems such as an Mo dimer in Au and an Re stripe in Cu are among the most promising top-stable candidates on the activity heatmap. The metal edge of MoS_2, an active site known for being an excellent electrocatalyst for the hydrogen evolution reaction, is also, notably, among the best candidate catalyst systems in our study.[31]

Another important finding (see Fig. 3A) is that the investigated catalyst systems appear to deviate increasingly from the ideal scaling line towards the stepped transition metal scaling line as $2E_N$ becomes more negative. Most points with $2E_N > 2$ eV fall on or close to ideal scaling, which is consistent with results on the less reactive rutile oxides[10,14] described by Vojvodic *et al.* Meanwhile, most points with $2E_N <$ -2 eV are close to the stepped transition metal scaling line. In the intermediate region (-2 eV $< 2E_N <$ 2 eV), the rate of deviation from ideal scaling appears to be system-dependent, and there is considerable scatter, with some points in the region of high rate and others on or above the stepped transition metal scaling line (lower rate).

To better understand the non-linearity in scaling observed here, E_{N-N} for the small reactive transition metal clusters in otherwise unreactive lattices, a subset of the systems

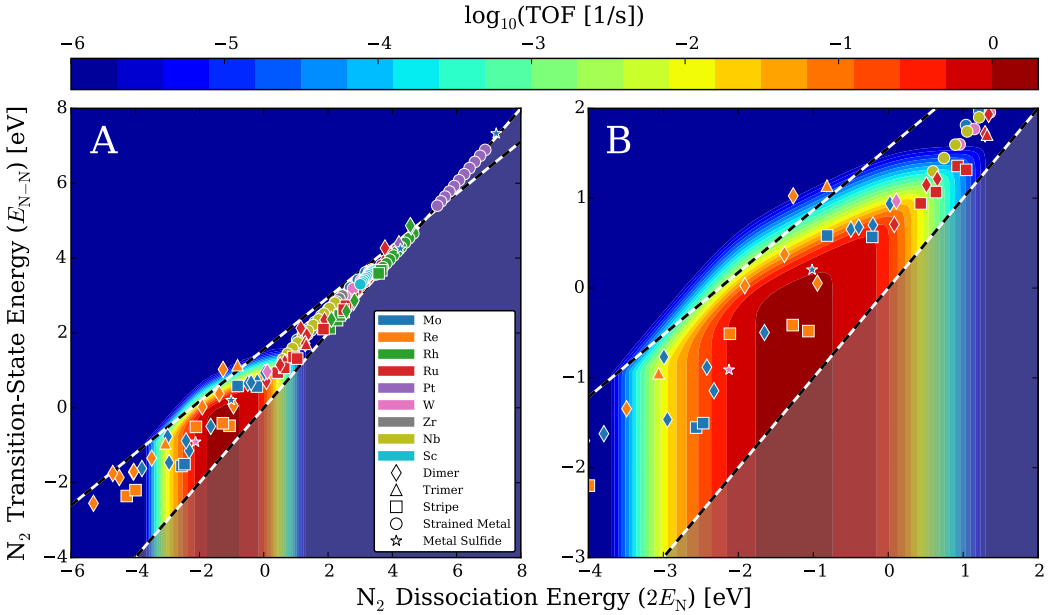

Figure 3: E_{N-N} vs. $2E_N$ results for various top-stable systems overlaid on the 2-D activity heatmap shown in Figure 2 (steady-state TOF to NH_3, computed at a temperature of 673 K, a total pressure of 100 bar, a stoichiometric ratio of H_2 to N_2 (3:1), and 10 percent conversion to NH_3). Panels (A) and (B) represent the same data, but (A) depicts a much wider energy space than (B).

considered, is compared to the transition-state N-N separation distance, a geometric property, in Fig. 4. There is a strong correlation between E_{N-N} and the distance between N atoms in the transition-state - materials with a more positive E_{N-N} (less reactive) have transition-states that more closely resemble the final dissociated state (larger N-N bond distance). Since the origin of transition-state scaling is the similarity in surface bonding of the transition-state and the final dissociated state, it is reasonable that the less reactive materials most closely obey linear scaling with a slope of 1 and an intercept of 0. More reactive materials have transition-states that more closely resemble an adsorbed N_2 molecule, the energy of which has a much more shallow dependence on $2E_N$ (slope significantly less than 1).[30] Thus, the deviation in scaling seen in these systems arises from the transition-state changing from "final-state like" to "initial-state like" as the catalyst becomes more reactive. Variations in transition-state bond distances have also previously been used to describe the non-linearity of transition-state scaling by Plessow *et al.*[32] Since the geometry of the system

has a significant impact on the N-N bond distance, it is not surprising that different systems deviate from scaling at different values of $2E_{\mathrm{N}}$. This explains some of the scatter seen at intermediate values of $2E_{\mathrm{N}}$ in Fig. 3.

To confirm the validity of the SS model, the full pathway for NH_3 production on one of the most promising candidate materials in this study is considered. The free energy diagram for NH_3 production on an Re stripe in Cu is shown in Fig. 5. The explicitly calculated transition-state for each step in the pathway can be compared to the corresponding linear BEP scaling equation for the step on transition metals.[28,33] While $E_{\mathrm{N-N}}$ is considerably lower than would be predicted for the transition metals (shown in red), the transition-state energy for the various hydrogenation steps are consistent with the scaling equations. This suggests that the $E_{\mathrm{N-N}}$ vs. E_{N} scaling is the only scaling relationship that is significantly altered for these top-stable systems, and thus that the overall reaction rates of the ammonia synthesis pathway would not be inhibited by perturbations to the energetics of hydrogenation steps.

Finally, Fig. 6 demonstrates the impact that an improvement in N-N transition-state scaling can have on the pressure requirements for thermochemical ammonia synthesis. From Fig. 3, the Re in Cu system exhibits a rate roughly two orders of magnitude higher than that represented by the peak of the stepped transition metal activity heatmap under the same temperature, pressure, and conversion. This result is reflected in the one-dimensional projection of the SS heatmap along the ideal and stepped transition metal scaling lines, as shown in Fig. 6B. To address how significantly the temperature and pressure requirements can be lowered such that the rate of the Re in Cu system matches the rates currently obtained on the best stepped transition-metal surfaces, we calculate the rate for the Re in Cu system from the SS model as a function of temperature and pressure in Fig. 6A. The optimal rate for a pure transition metal from the transition metal scaling activity heatmap can be achieved in the Re in Cu system with a substantially lower pressure (approximately 25 bar) and marginally lower temperature (600 K). This improvement in scaling corresponds to a roughly four-fold reduction in pressure, which might significantly decrease the costs of

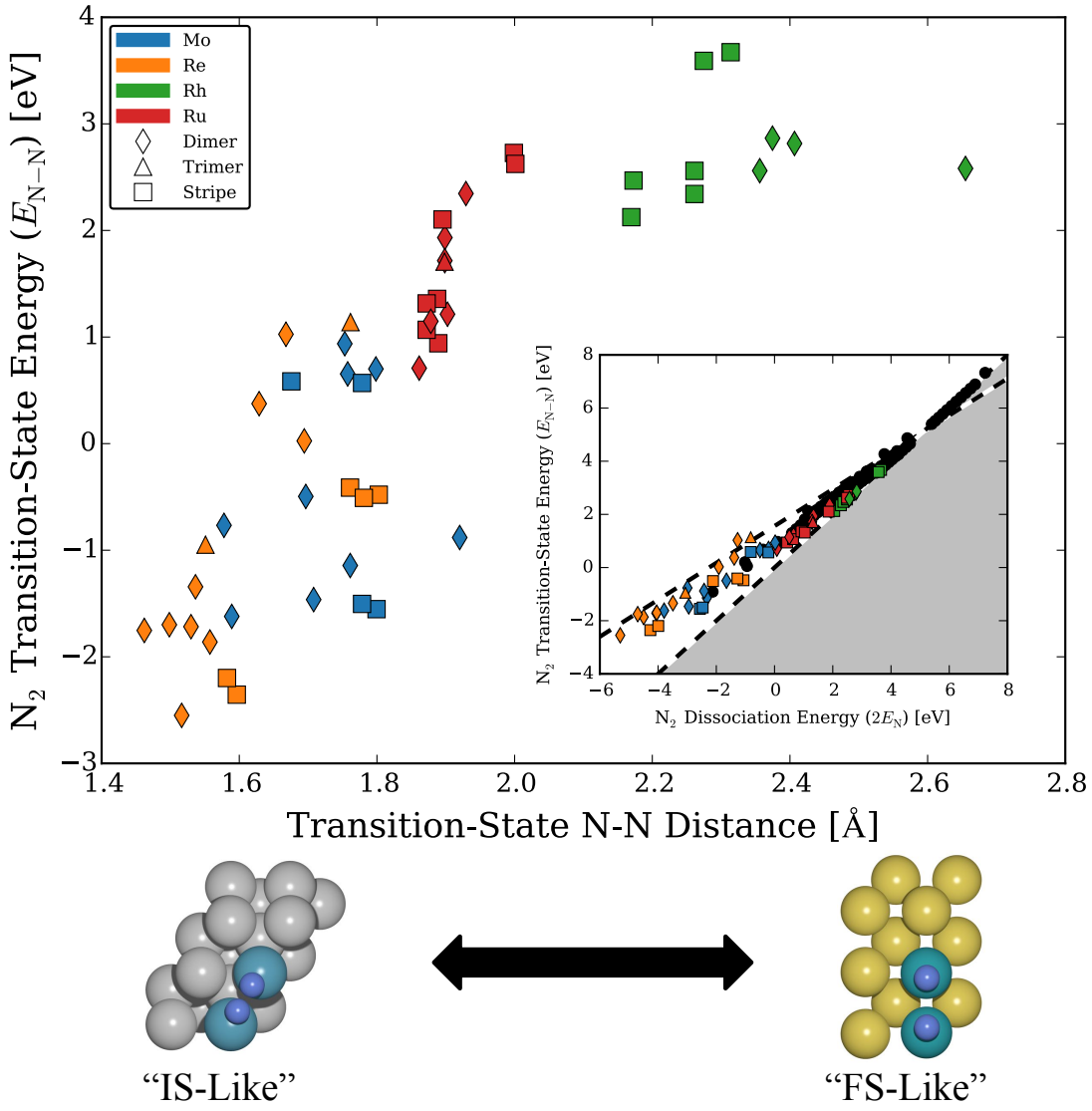

Figure 4: A plot of E_{N-N} vs. transition-state N-N separation distance for various top-stable systems (E_{N-N} vs. $2E_N$ data from Figure 3 is shown for comparison in the inset). Images are shown of a rhenium dimer in a silver (111) lattice (a representative "initial-state like" transition-state) and a rhodium dimer in a gold (100) lattice (a representative "final-state like" transition-state).

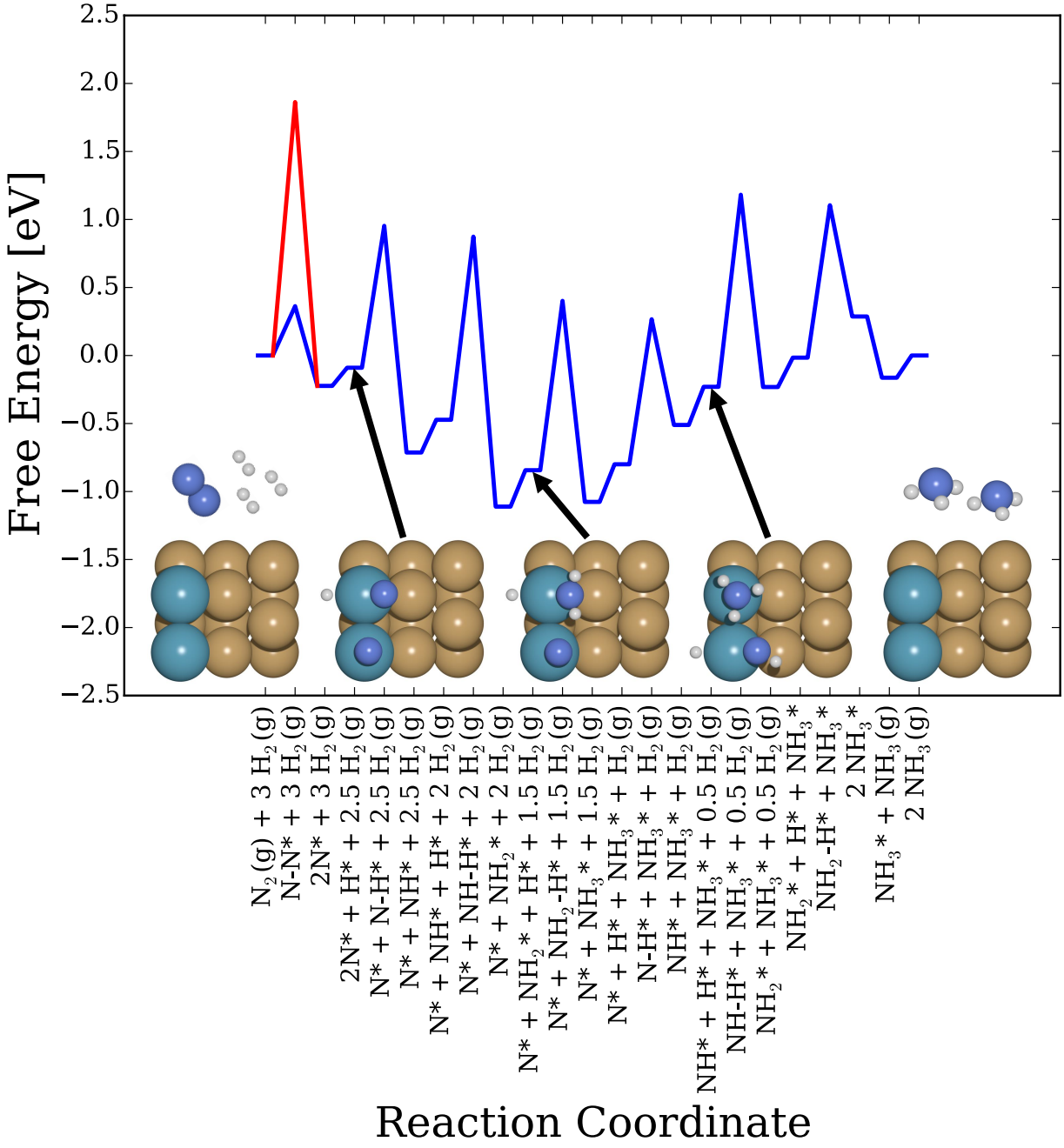

Figure 5: Free energy diagram, shown in blue, for NH_3 production on a rhenium stripe in copper (211), computed at a temperature of 673 K, a total pressure of 100 bar, a stoichiometric ratio of H_2 to N_2 (3:1), and 10 percent conversion to NH_3. The scaled barrier for N_2 dissociation on a stepped transition metal surface with a comparable dissociation energy is shown in red. Also displayed are top-view images of selected states along the reaction coordinate.

ammonia production via the Haber-Bosch process.

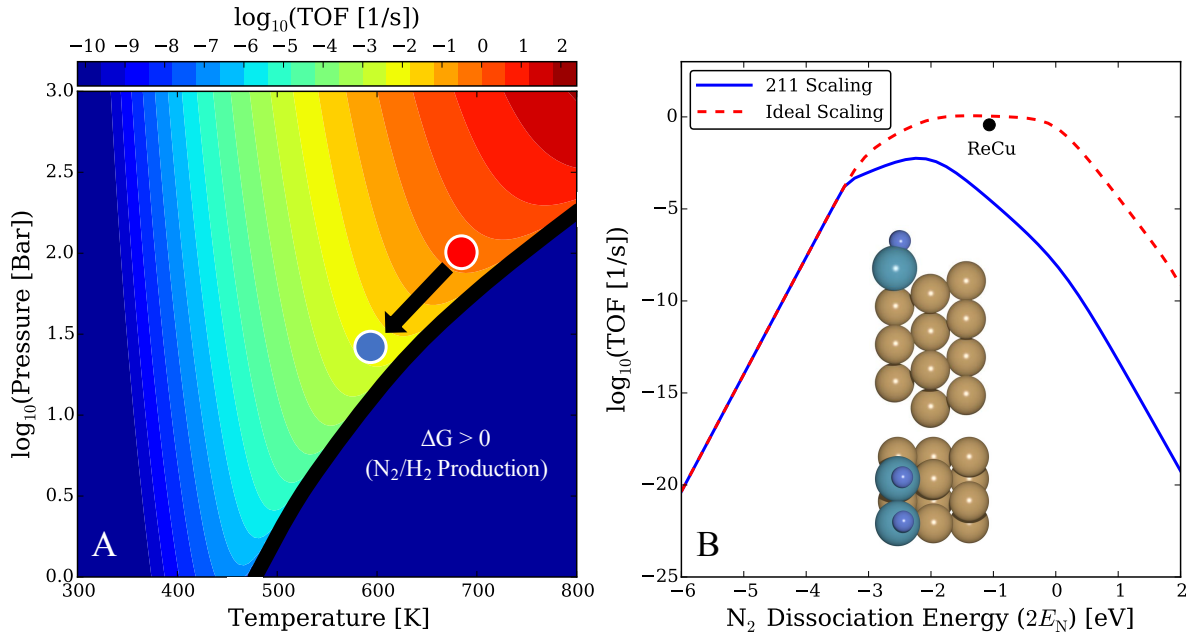

Figure 6: (A) The steady-state TOF to NH_3 for a rhenium stripe in copper (211), shown as a function of temperature and pressure, at a constant stoichiometric ratio of H_2 to N_2 (3:1), and 10 percent conversion to NH_3. The red circle represents current industrial conditions (T = 673 K and P = 100 bar), while the blue circle represents the current industrial rate, obtainable under more benign conditions (T = 600 K and P = 25 bar). (B) A 1-D projection of the steady-state activity heatmap from Figures 2-3 taken along the ideal and stepped transition metal scaling lines, with the result for a rhenium stripe in copper (211) shown explicitly.

4 Conclusions and Outlook

In this study, we use DFT calculations to describe how a new type of model active site could exhibit improved ammonia synthesis activity by forcing dissociative adsorption of nitrogen into singly-coordinated adsorption geometries. Our results show that materials containing such an active site (involving at least two isolated reactive metal atoms in a non-reactive framework) follow a substantially more favorable transition-state scaling relationship between E_{N-N} and $2E_N$, leading to an enhancement in predicted activity and substantially lower pressure requirements. Some of the systems explored here resemble systems proposed

by Martirez *et al.* for an alternative approach toward low-temperature NH_3 synthesis, in which sunlight converted into surface plasmon resonances can reduce the barrier for N_2 dissociation on reactive Mo sites doped in unreactive Au nanoparticles.[34] The systems presented here may also be interesting candidates for this new technique. It is important to note that the synthesis of new catalytic materials with a top-stable site is likely to be a significant challenge; however, some progress has been made. Yan *et al.* have recently demonstrated the precise synthesis of platinum dimers on graphene,[35] and Yardimci *et al.* have generated rhodium dimers on MgO that are active for ethylene hydrogenation,[36] indicating that the synthesis of these top-stable active sites may become more feasible in the future. Furthermore, some known systems, like metal edges of transition metal sulfides, are known to exhibit the geometry of interest. To identify other candidates for experiments, it may also be beneficial to search for complex binary or ternary materials that are known to contain this type of active site geometry and are stable under ammonia synthesis conditions.

Acknowledgement

This work was supported by a research grant (9455) from VILLUM FONDEN. The authors acknowledge support from the U.S. Department of Energy Office of Basic Energy Sciences to the SUNCAT Center for Interface Science and Catalysis. B.A.R. was supported by the NSF GFRP, grant number DGE-1656518.

Supporting Information Available

The Supporting Information contains the geometry and energetics for the various systems explored in this study.

This material is available free of charge via the Internet at `http://pubs.acs.org/`.

References

(1) Smil, V. Detonator of the Population Explosion. *Nature* **1999**, *400*, 415.

(2) Erisman, J. W.; Sutton, M. A.; Galloway, J.; Klimont, Z.; Winiwarter, W. How a Century of Ammonia Synthesis Changed the World. *Nat. Geosci.* **2008**, *1*, 636–639.

(3) Emmett, P.; Brunauer, S. The Adsorption of Nitrogen by Iron Synthetic Ammonia Catalysts. *J. Am. Chem. Soc.* **1934**, *56*, 35–41.

(4) Boudart, M. Kinetics and Mechanism of Ammonia Synthesis. *Catal. Rev.: Sci. Eng.* **1981**, *23*, 1–15.

(5) Dahl, S.; Taylor, P. A.; Törnqvist, E.; Chorkendorff, I. The Synthesis of Ammonia Over a Ruthenium Single Crystal. *J. Catal.* **1998**, *178*, 679–686.

(6) Logadottir, A.; Rod, T. H.; Nørskov, J. K.; Hammer, B.; Dahl, S.; Jacobsen, C. The Brønsted–Evans–Polanyi Relation and the Volcano Plot for Ammonia Synthesis Over Transition Metal Catalysts. *J. Catal.* **2001**, *197*, 229–231.

(7) Schlögl, R. Catalytic Synthesis of Ammonia-A "Never-Ending Story"? *Angew. Chem., Int. Ed.* **2003**, *42*, 2004–2008.

(8) Honkala, K.; Hellman, A.; Remediakis, I.; Logadottir, A.; Carlsson, A.; Dahl, S.; Christensen, C. H.; Nørskov, J. K. Ammonia Synthesis from First-Principles Calculations. *Science* **2005**, *307*, 555–558.

(9) Ertl, G. Surface Science and Catalysis-Studies on the Mechanism of Ammonia Synthesis: The P. H. Emmett Award Address. *Catal. Rev.* **2006**, *21*, 201–223.

(10) Vojvodic, A.; Medford, A. J.; Studt, F.; Abild-Pedersen, F.; Khan, T. S.; Bligaard, T.; Nørskov, J. K. Exploring the Limits: A Low-Pressure, Low-Temperature Haber-Bosch Process. *Chem. Phys. Lett.* **2014**, *598*, 108–112.

(11) Delmer, D. P. Agriculture in the Developing World: Connecting Innovations in Plant Research to Downstream Applications. *Proc. Natl. Acad. Sci. U. S. A.* **2005**, *102*, 15739–15746.

(12) Nørskov, J. K.; Bligaard, T.; Hvolbæk, B.; Abild-Pedersen, F.; Chorkendorff, I.; Christensen, C. H. The Nature of the Active Site in Heterogeneous Metal Catalysis. *Chem. Soc. Rev.* **2008**, *37*, 2163–2171.

(13) Munter, T. R.; Bligaard, T.; Christensen, C. H.; Nørskov, J. K. BEP Relations for N2 Dissociation Over Stepped Transition Metal and Alloy Surfaces. *Phys. Chem. Chem. Phys.* **2008**, *10*, 5202–5206.

(14) Vojvodic, A.; Calle-Vallejo, F.; Guo, W.; Wang, S.; Toftelund, A.; Studt, F.; Martinez, J. I.; Shen, J.; Man, I. C.; Rossmeisl, J.; Bligaard, T.; Nørskov, J. K.; Abild-Pedersen, F. On the Behavior of Brønsted-Evans-Polanyi Relations for Transition Metal Oxides. *J. Chem. Phys.* **2011**, *134*, 1–8.

(15) Bahn, S. R.; Jacobsen, K. W. An Object-Oriented Scripting Interface to a Legacy Electronic Structure Code. *Comput. Sci. Eng.* **2002**, *4*, 56–66.

(16) Wellendorff, J.; Lundgaard, K. T.; Møgelhøj, A.; Petzold, V.; Landis, D. D.; Nørskov, J. K.; Bligaard, T.; Jacobsen, K. W. Density Functionals for Surface Science: Exchange-Correlation Model Development with Bayesian Error Estimation. *Phys. Rev. B* **2012**, *85*, 1–23.

(17) Monkhorst, H. J.; Pack, J. D. Special Points for Brillouin-Zone Integrations. *Phys. Rev. B* **1976**, *13*, 5188–5192.

(18) Mavrikakis, M.; Hammer, B.; Nørskov, J. K. Effect of Strain on the Reactivity of Metal Surfaces. *Phys. Rev. Lett.* **1998**, *81*, 2819–2822.

(19) Sholl, D.; Steckel, J. A. *Density Functional Theory: A Practical Introduction*; John Wiley & Sons, 2011; pp 56–59.

(20) Alavi, A.; Hu, P.; Deutsch, T.; Silvestrelli, P. L.; Hutter, J. CO Oxidation on Pt (111): An Ab Initio Density Functional Theory Study. *Phys. Rev. Lett.* **1998**, *80*, 3650–3653.

(21) Liu, Z.-P.; Hu, P. General Rules for Predicting Where a Catalytic Reaction Should Occur on Metal Surfaces: A Density Functional Theory Study of C-H and C-O Bond Breaking/Making on Flat, Stepped, and Kinked Metal Surfaces. *J. Am. Chem. Soc.* **2003**, *125*, 1958–1967.

(22) Yu, L.; Abild-Pedersen, F. Bond Order Conservation Strategies in Catalysis Applied to the NH3 Decomposition Reaction. *ACS Catal.* **2016**, *7*, 864–871.

(23) Medford, A. J.; Shi, C.; Hoffmann, M. J.; Lausche, A. C.; Fitzgibbon, S. R.; Bligaard, T.; Nørskov, J. K. CatMAP: A Software Package for Descriptor-Based Microkinetic Mapping of Catalytic Trends. *Catal. Lett.* **2015**, *145*, 794–807.

(24) Medford, A. J.; Wellendorff, J.; Vojvodic, A.; Studt, F.; Abild-Pedersen, F.; Jacobsen, K. W.; Bligaard, T.; Nørskov, J. K. Assessing the Reliability of Calculated Catalytic Ammonia Synthesis Rates. *Science* **2014**, *345*, 197–200.

(25) Medford, A. J.; Vojvodic, A.; Hummelshøj, J. S.; Voss, J.; Abild-Pedersen, F.; Studt, F.; Bligaard, T.; Nilsson, A.; Nørskov, J. K. From the Sabatier Principle to a Predictive Theory of Transition-Metal Heterogeneous Catalysis. *J. Catal.* **2015**, *328*, 36–42.

(26) Cheng, J.; Hu, P. Utilization of the Three-Dimensional Volcano Surface to Understand the Chemistry of Multiphase Systems in Heterogeneous Catalysis. *J. Am. Chem. Soc.* **2008**, *130*, 10868–10869.

(27) Xu, Y.; Lausche, A. C.; Wang, S.; Khan, T. S.; Abild-Pedersen, F.; Studt, F.;

Nørskov, J. K.; Bligaard, T. In Silico Search for Novel Methane Steam Reforming Catalysts. *New J. Phys.* **2013**, *15*, 1–18.

(28) Wang, S.; Petzold, V.; Tripkovic, V.; Kleis, J.; Howalt, J. G.; Skulason, E.; Fernandez, E.; Hvolbæk, B.; Jones, G.; Toftelund, A.; Falsig, H.; Björketun, M.; Studt, F.; Abild-Pedersen, F.; Rossmeisl, J.; Nørskov, J. K.; Bligaard, T. Universal Transition State Scaling Relations for (De)Hydrogenation Over Transition Metals. *Phys. Chem. Chem. Phys.* **2011**, *13*, 20760–20765.

(29) Montoya, J. H.; Tsai, C.; Vojvodic, A.; Nørskov, J. K. The Challenge of Electrochemical Ammonia Synthesis: A New Perspective on the Role of Nitrogen Scaling Relations. *ChemSusChem* **2015**, *8*, 2180–2186.

(30) Skulason, E.; Bligaard, T.; Gudmundsdóttir, S.; Studt, F.; Rossmeisl, J.; Abild-Pedersen, F.; Vegge, T.; Jónsson, H.; Nørskov, J. K. A Theoretical Evaluation of Possible Transition Metal Electro-Catalysts for N2 Reduction. *Phys. Chem. Chem. Phys.* **2012**, *14*, 1235–1245.

(31) Tsai, C.; Abild-Pedersen, F.; Nørskov, J. K. Tuning the MoS2 Edge-Site Activity for Hydrogen Evolution via Support Interactions. *Nano Lett.* **2014**, *14*, 1381–1387.

(32) Plessow, P. N.; Abild-Pedersen, F. Examining the Linearity of Transition State Scaling Relations. *J. Phys. Chem. C* **2015**, *119*, 10448–10453.

(33) Wang, S.; Temel, B.; Shen, J.; Jones, G.; Grabow, L. C.; Studt, F.; Bligaard, T.; Abild-Pedersen, F.; Christensen, C. H.; Nørskov, J. K. Universal Brønsted-Evans-Polanyi Relations for C-C, C-O, C-N, N-O, N-N, and O-O Dissociation Reactions. *Catal. Lett.* **2011**, *141*, 370–373.

(34) Martirez, J. M. P.; Carter, E. A. Prediction of a Low-Temperature N2 Dissociation Catalyst Exploiting Near-IR–to–Visible Light Nanoplasmonics. *Sci. Adv.* **2017**, *3*, 1–10.

(35) Yan, H.; Lin, Y.; Wu, H.; Zhang, W.; Sun, Z.; Cheng, H.; Liu, W.; Wang, C.; Li, J.; Huang, X.; Yao, T.; Yang, J.; Wei, S.; Lu, J. Bottom-up Precise Synthesis of Stable Platinum Dimers on Graphene. *Nat. Commun.* **2017**, *8*, 1–11.

(36) Yardimci, D.; Serna, P.; Gates, B. C. Surface-Mediated Synthesis of Dimeric Rhodium Catalysts on MgO: Tracking Changes in the Nuclearity and Ligand Environment of the Catalytically Active Sites by X-ray Absorption and Infrared Spectroscopies. *Chem. - Eur. J.* **2013**, *19*, 1235–1245.

Graphical TOC Entry